

TEM investigation of the structure of deformation-induced antiphase boundary faults in Ni₃Al

Christian Rentenberger,* Thomas Waitz, and H. Peter Karnthaler

Institute of Materials Physics, University of Vienna, Boltzmanngasse 5, A-1090 Vienna, Austria

(Received 4 October 2002; published 21 March 2003)

Transmission electron microscopy (TEM) methods were used to analyze the deformation-induced antiphase boundary (APB) tubes in a Ni₃Al single crystal. A high density of tubes is observed after room-temperature deformation showing strong contrasts in some fundamental reflections. This is not expected from a hard sphere model of the APB faults bounding the tubes since in this case the APB faults are just chemical faults (displacement vector $\vec{R}_C = 1/2\langle 110 \rangle$). The TEM analysis shows unambiguously that the APB faults contain a small additional structural displacement vector \vec{R}_S . \vec{R}_S lies in the plane of the fault and is perpendicular to \vec{R}_C .

DOI: 10.1103/PhysRevB.67.094109

PACS number(s): 68.37.Lp, 61.72.Nn

I. INTRODUCTION

Transmission electron microscopy (TEM) investigations of $L1_2$ -ordered alloys show the occurrence of deformation-induced antiphase boundary (APB) tubes aligned along the close-packed direction $\langle 110 \rangle$. These elongated defects consist of APB faults on different planes bounding a tube. They can be formed by different mechanisms: e.g., by the movement of superlattice dislocations with nonaligned jogs,^{1,2} by the annihilation of superlattice screw dislocations, or by the double cross-slip of superlattice screw dislocations.² The influence of the APB tubes on work hardening in ordered alloys was discussed by several authors.¹⁻⁴

Since antiphase boundaries disturb the chemical order across the interface, APB tubes can be imaged using superlattice reflections.⁵ No contrast is expected in fundamental reflections \vec{g} since in this case the phase factor $\alpha = 2\pi\vec{g}\cdot\vec{R}_C$ equals $2\pi n$ (n , integer) with $\vec{R}_C = 1/2\langle 110 \rangle$ (\vec{R}_C , displacement vector of the APB fault as obtained from the hard sphere model causing a pure chemical fault in the ordered structure). Contrary to this, several authors^{4,6-11} showed that APB tubes lead to contrast in TEM images when fundamental reflections are used.

To explain this unexpected contrast different models of APB tubes were proposed in the literature that contain additional displacement vectors not resulting from the hard sphere model. Sun⁶ proposed a relaxation component that originates from a surface tension of the APB tube. Ngan *et al.*⁷ suggested a relaxation model that is based on the TEM observations of grown-in thermal APB faults in annealed samples. Both models contain vector components additional to \vec{R}_C that are perpendicular to the planes of the APB faults. Contrary to this, several atomistic calculations indicate a supplementary structural displacement vector \vec{R}_S lying in the fault planes. Such a component was deduced from calculating the atomic displacements caused by a tube using embedded atom methods.¹² In the case of single APB faults both pair-potential calculations¹³⁻¹⁵ and *ab initio* calculations¹⁶ lead also to an additional component in the fault plane. Experimental evidence whether the additional components of the APB faults are perpendicular or parallel to the fault plane is still missing. It is therefore the aim of this paper to carry

out a careful analysis to answer this question.

II. EXPERIMENTAL PROCEDURE

Single crystals of binary Ni₃Al (77 at. % Ni, 23 at. % Al) were grown under vacuum using a modified Bridgman technique and were homogenized at 1200 °C for 140 h to reduce their dendritic structure. A compression sample ($3 \times 3 \times 7$ mm³) oriented for single slip (compression axis parallel $[\bar{1}23]$) was deformed at room temperature (RT) at about 4% true strain (primary Burgers vector $\vec{b} = \pm[10\bar{1}]$). The specimen was sectioned parallel to the primary octahedral plane (foil normal $\vec{FN} \approx [111]$) by spark erosion. Small disks (1.4 mm in diameter) were dimpled electrochemically by a jet procedure (120 ml perchloric acid, 320 ml butoxyethanol, 560 ml methanol, 50 ml glycerol) at RT and TEM foils were prepared by electropolishing them in a solution of 0.5% perchloric acid in methanol at -70 °C.

The TEM investigation was carried out using an acceleration voltage of 150 kV in a Philips CM30ST electron microscope equipped with a Gatan slow-scan charge-coupled-device (CCD) camera. Bright-field images and pseudo-weak-beam dark-field images (using deviation parameters $|\vec{s}_g| < 0.2$ nm⁻¹) were taken. For the dark-field images the reflection vectors $\vec{g} = \pm[1\bar{1}1]$ (perpendicular to \vec{b}), $\vec{g} = [20\bar{2}]$ (parallel to \vec{b}), and $\vec{g} = \langle 113 \rangle$ were used applying $\vec{g}(-\vec{g})$ ($|\vec{s}_g| = -0.07$ nm⁻¹), $\vec{g}(3\vec{g})$ ($|\vec{s}_g| = 0.19$ nm⁻¹), and $\vec{g}(2\vec{g})$ ($|\vec{s}_g| = 0.13$ nm⁻¹) diffraction conditions, respectively. Using the CCD camera the maximum intensity I_{max} of the tubes was measured and normalized to the background I_{back} , giving the contrast $C = (I_{max} - I_{back})/I_{back}$ of the tubes. Finally, TEM contrast simulations of the tubes were performed using the many-beam program (CUFOUR) developed by Schäublin and Stadelmann.¹⁷

III. RESULTS

A. TEM results

Figure 1 shows a TEM bright-field image of Ni₃Al deformed at RT using the fundamental reflection $\vec{g} = [1\bar{1}1]$ that is perpendicular to the Burgers vector \vec{b} of the primary su-

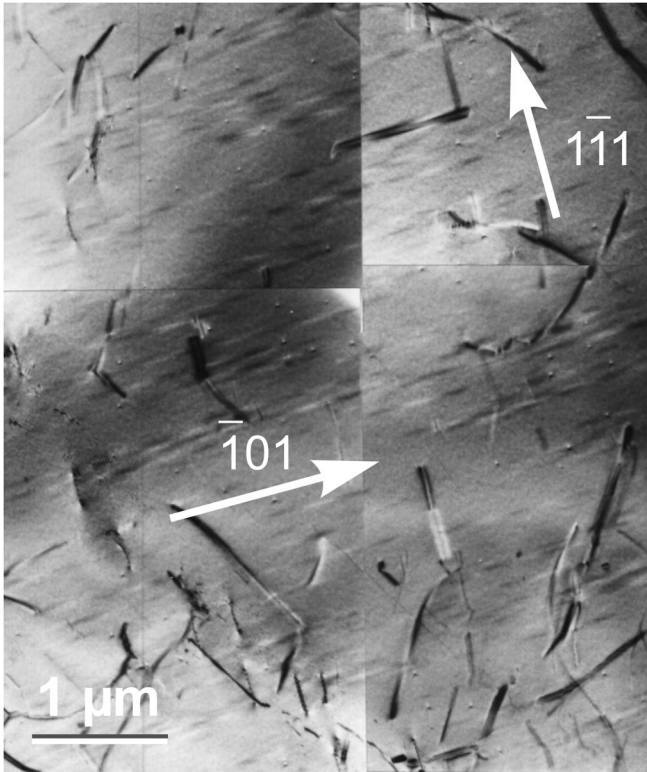


FIG. 1. TEM bright-field image of Ni_3Al single crystal oriented for single slip and deformed at room temperature ($\vec{g}=[1\bar{1}1]$, $\vec{FN} \approx [111]$, $\vec{BD} \approx [121]$ Ref. 19). A high density of APB tubes is observed that are aligned along $\vec{b} = \pm[10\bar{1}]$ (depth oscillations of adjacent tubes can cause the visual impression that the direction of the tubes deviates from \vec{b}). The primary superlattice dislocations show residual contrast only since $\vec{g} \cdot \vec{b} = 0$.

perlatice dislocations. A high density of APB tubes is observed. The tubes are running parallel to \vec{b} showing depth oscillations (\vec{FN} deviates about 4° from $[111]$). Primary screw dislocations are rare, and the dislocation structure consists mainly of primary edge dislocations¹⁸ showing residual contrast only when \vec{g} perpendicular \vec{b} is used.

Using (pseudo-)weak-beam images the contrast of the tubes is enhanced (cf. Fig. 2). The tubes show depth oscillations and depending on the sign of \vec{g} ($|\vec{s}_g|$ constant) the outer fringes show all either dark (cf. Fig. 2(a), $\vec{g}=[1\bar{1}1]$) or bright (cf. Fig. 2(b), $\vec{g}=[\bar{1}1\bar{1}]$) contrast. In Figs. 2(c)–2(e) three different $\langle 113 \rangle$ reflections were applied. The reflection vector $\vec{g}=[\bar{1}3\bar{1}]$ is running perpendicular to the line of the tubes and gives stronger contrast [$C=0.63$ as measured on the tube marked by T in Fig. 2(c)] as compared to $\vec{g}=[\bar{3}11]$ [$C=0.45$; cf. Fig. 2(d)]. Using $\vec{g}=[31\bar{1}]$ no contrast was observed [cf. Fig. 2(e)]; this result is unchanged even when the TEM foil is tilted about 35° ($\vec{BD} \approx [011]$ to $\approx [114]$). Finally, the tubes are also out of contrast in $\vec{g}=[20\bar{2}]$ which lies parallel to the line of the tubes [cf. Fig. 2(f)]. The results are listed in Table I. (It should be noted that

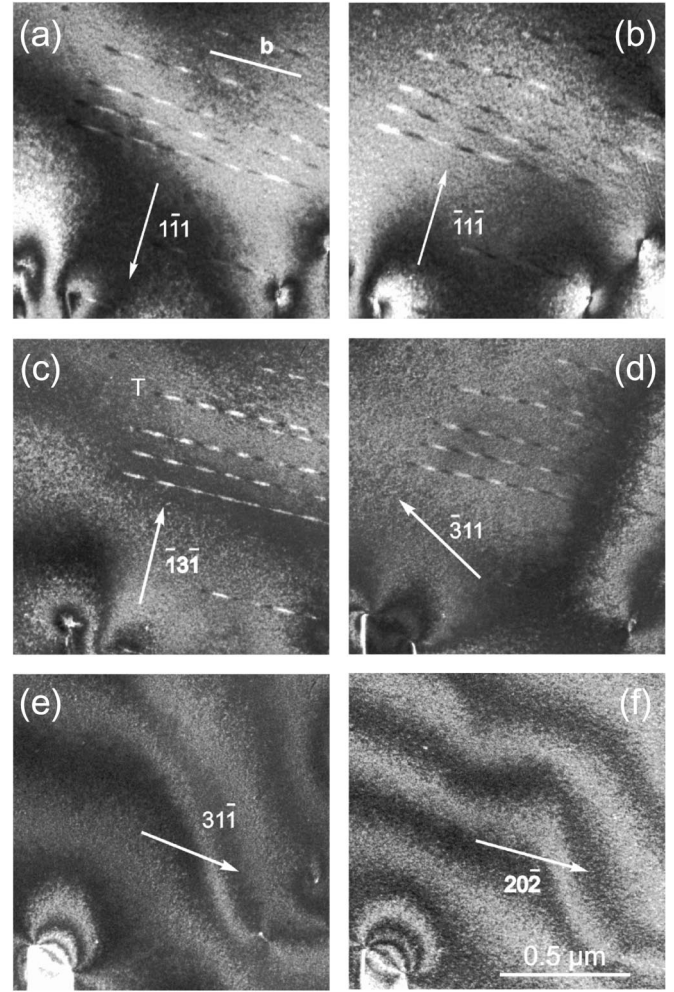


FIG. 2. TEM contrast analysis of APB tubes using different reflection vectors (pseudo-weak-beam images of the same area; tube T was used to measure the contrast). (a) $\vec{g}=[111]$, $\vec{BD} \approx [121]$. The tubes are in contrast. (b) $\vec{g}=[\bar{1}1\bar{1}]$, $\vec{BD} \approx [121]$. The contrast is inverted since the edge fringes show bright contrast. The tubes are visible in both (c) ($\vec{g}=[\bar{1}3\bar{1}]$, $\vec{BD} \approx [323]$) and (d) ($\vec{g}=[\bar{3}11]$, $\vec{BD} \approx [112]$) whereas they are out of contrast in (e) ($\vec{g}=[31\bar{1}]$, $\vec{BD} \approx [011]$) and (f) ($\vec{g}=[20\bar{2}]$, $\vec{BD} \approx [111]$).

TABLE I. List of the experimental results of the TEM images shown in Fig. 2. The contrast of the APB tubes correlates with $\vec{g} \cdot \vec{R}_S$ (\vec{g} diffraction vector, $|\vec{s}_g|$ deviation parameter, $\vec{R}_S = (1/50)[1\bar{2}1]$).

Fig. 2	\vec{g}	$ \vec{s}_g $	Contrast	$\vec{g} \cdot \vec{R}_S$
(a)	$1\bar{1}1$	-0.07	Yes	0.08
(b)	$\bar{1}1\bar{1}$	-0.07	Yes	-0.08
(c)	$\bar{1}3\bar{1}$	0.13	Yes, strong	0.16
(d)	$\bar{3}11$	0.13	Yes	0.08
(e)	$31\bar{1}$	0.13	No	0
(f)	$20\bar{2}$	0.19	No	0

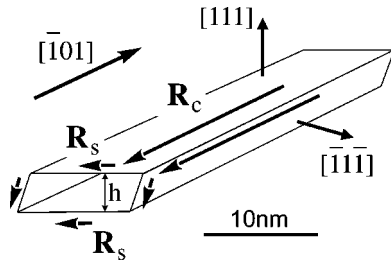


FIG. 3. Sketch of an APB tube bounded by four interfaces on $\{111\}$ planes. The chemical displacement vector \vec{R}_C and the additional structural displacement vector \vec{R}_S of the fault planes are indicated.

the contrast features are similar in the corresponding bright-field images.)

B. Analysis of the additional structural displacement vector

$$\vec{R}_S$$

The results of Table I can be used to determine the displacement vector of the APB's bounding the tubes. It is assumed that their total displacement vector $\vec{R} = \vec{R}_C + \vec{R}_S$. Using fundamental reflection vectors \vec{g} the additional displacement \vec{R}_S causes a phase shift $\alpha = 2\pi\vec{g} \cdot \vec{R}_S$ that differs from $2\pi n$. Therefore contrast from the tubes is expected in fundamental reflections, as observed in Figs. 2(a)–2(d). However, the contrast vanishes when \vec{g} is perpendicular to \vec{R}_S , i.e., $\vec{g} \cdot \vec{R}_S = 0$. Since the tubes show no contrast using both $\vec{g} = [31\bar{1}]$ and $\vec{g} = [20\bar{2}]$ [cf. Figs. 2(e) and 2(f)], it is concluded that \vec{R}_S is parallel to $[31\bar{1}] \times [20\bar{2}]$; therefore the additional structural displacement vector \vec{R}_S is parallel to $\pm[1\bar{2}1]$ which lies in the (111) plane of the APB fault. High contrast can be obtained when α is large as in the case of $\vec{g} = [1\bar{3}\bar{1}]$. Since the outer fringes show all the same contrast (either bright or dark depending on the sign of both \vec{g} and $|\vec{s}_g|$), the supplementary displacement vectors of the faults shown in Fig. 2 have all the same sign.

C. Comparison with image simulations

A model of an APB tube running along $[\bar{1}01]$ is sketched in Fig. 3. The tube is formed by four APB faults lying on two sets of $\{111\}$ planes: (111) fault ribbons with a constant width (10 nm) and $(\bar{1}\bar{1}\bar{1})$ fault ribbons whose width was varied, leading to different heights h of the tube. For the calculations it was assumed that all the $\{111\}$ faces contain the same chemical faults $\vec{R}_C = 1/2[10\bar{1}]$ whereas two different assumptions for \vec{R}_S were made.

First, as sketched in Fig. 3, \vec{R}_S is contained in the plane of the fault (parallel to $[1\bar{2}1]$ on the (111) faces and according to symmetry parallel to $[\bar{1}\bar{2}\bar{1}]$ on the side faces $(\bar{1}\bar{1}\bar{1})$). It should be noted that \vec{R}_S has the same sign on parallel faces since the reversion of the sign of \vec{R}_S would lead to a different structural defect. (In this respect the situation is analogous to

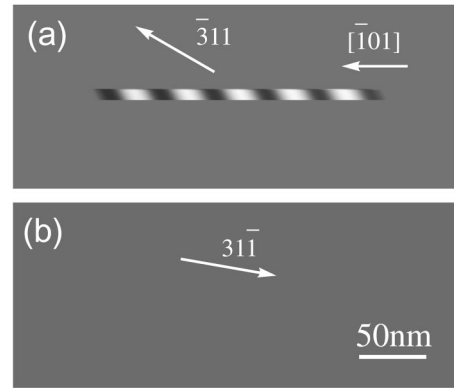


FIG. 4. Image simulation of an APB tube containing a structural displacement vector $\vec{R}_S = (1/50)[1\bar{2}\bar{1}]$ on the (111) plane. In (a) the tube shows strong contrast using $\vec{g} = [3\bar{1}\bar{1}]$ ($\vec{B}\vec{D} = [112]$) in agreement with the TEM image of Fig. 2(d). In (b) the contrast of the tube vanishes completely (since $\vec{g} = [3\bar{1}\bar{1}]$ is perpendicular to \vec{R}_S , $\vec{B}\vec{D} = [011]$) which is again in agreement with the TEM image of Fig. 2(e).

that of overlapping intrinsic stacking faults in fcc structures.) The length of \vec{R}_S was assumed to be rather small ($\vec{R}_S = (1/50)\langle 112 \rangle$) as proposed by Schoeck *et al.*¹⁶ In Fig. 4(a) $\vec{g} = [3\bar{1}\bar{1}]$ was used and both the simulation and the experimental image [cf. Fig. 2(d)] show oscillations of similar contrast. When $\vec{g} = [3\bar{1}\bar{1}]$ is applied the faults on the (111) planes show no contrast in agreement with the experiment [cf. Figs. 2(e) and 4(b)]. It should be noted that in Fig. 4 the height $h = 1$ nm and therefore the faults on $(\bar{1}\bar{1}\bar{1})$ planes are almost invisible. However, the side planes show up when $h > 1$ nm.

Second, \vec{R}_S was assumed to be normal to the fault planes having a similar length as proposed by Ngan *et al.*⁷ ($\vec{R}_S = (1/25)[111]$ for the (111) fault planes). In this case the simulation for $\vec{g} = [3\bar{1}\bar{1}]$ shows a strong contrast of the faults on (111) planes (cf. Fig. 5) which disagrees with the experimental TEM image [cf. Fig. 2(e)].

It should be mentioned that the contrast of the background of the simulated images is uniform whereas in the experimental images it is rather inhomogeneous which is caused by bend contours, contamination, and surface roughness.

IV. DISCUSSION

APB tubes show contrast in TEM micrographs using fundamental reflections (cf. Figs. 1 and 2) that is not expected

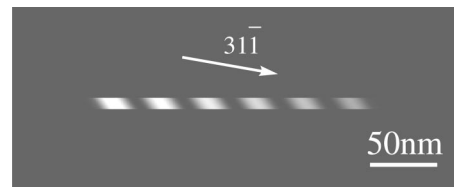


FIG. 5. Image simulation of an APB tube containing \vec{R}_S perpendicular to the planes of the APB fault. Contrary to the TEM image of Fig. 2(e) the APB tube shows strong contrast when $\vec{g} = [3\bar{1}\bar{1}]$ ($\vec{B}\vec{D} = [011]$).

(“forbidden”) on the basis of a hard sphere model. This unexpected contrast can be explained by a structural displacement vector \vec{R}_S . Contrary to this the method of imaging \vec{R}_C of the APB faults by superlattice reflections yields in the case of tubes only a very weak contrast (especially when h is small) since it results from two overlapping π faults (canceling their contrast). This might be the reason that the occurrence of a high density of tubes (as shown in Fig. 1) was not observed previously. Since tubes connected to glide dislocations (at jogs) have hardly been encountered in this study, it is concluded that the large density of tubes was formed by cross-slip and annihilation of screw dislocations.² This is in agreement with the observation that in specimens deformed at room temperature the structure is dominated by primary dislocations of near edge character whereas screws are rather rare.

The comparison of the experimental results with the simulated images (cf. Figs. 2 and 4) shows unambiguously that the structural displacement vector \vec{R}_S has no component perpendicular to the $\{111\}$ fault planes. Therefore the models of the tubes proposed by Sun⁶ and by Ngan *et al.*⁷ can be ruled out. It should be noted, however, that components perpendicular to the fault planes^{7,20} might occur in the case of APB faults in thermal equilibrium and grown-in APB faults since in these cases the antiphase boundaries are assumed to be extended perpendicular to the fault planes.²¹

The present result is in good agreement with calculations of the γ surface of Ni₃Al (Refs. 13 and 16) ($L1_2$ structure) that propose the minimum of the APB energy at a position shifted slightly along $[1\bar{2}1]$ from the position given by the hard sphere model. Although the sense of the displacement vector \vec{R}_S has not been determined experimentally, it is likely to be of a sign increasing the Al-Al spacing as resulting from the calculations. It should be mentioned that APB tubes in FeAl ($B2$ structure) show no contrast in fundamental reflections as observed by Chou and Hirsch²² since in this case the local minimum of the γ surface corresponds to the APB fault vector of the hard sphere model.²³

The image simulations show that strong contrast of APB faults arises in fundamental reflections even when \vec{R}_S is rather small. It should be noted that the invisibility criterion $\vec{g} \cdot \vec{R}_S = 0$ using $\vec{g} = [31\bar{1}]$ [cf. Fig. 4(b)] holds for the faces

of the tubes on the primary octahedral glide planes (top and bottom faces) only. When the side faces are assumed to lie also on the octahedral planes ($1\bar{1}1$), $\vec{g} \cdot \vec{R}_S \neq 0$. However, their contrast is almost invisible in agreement with the TEM images when the width of the side faces is less than about 1 nm. It should be mentioned that side faces lying on the cube cross-slip planes (010) would be out of contrast in any fundamental reflection since in this case the calculations indicate that no supplementary displacement vector should occur.^{12,24} When two inclined APB faults join up no stair-rod dislocation is necessary at the edge when they are formed by pure chemical faults \vec{R}_C . Contrary to this, when the APB faults contain an additional structural component \vec{R}_S a stair-rod dislocation has to be formed for topological reasons (as in the case of stacking faults). Since the magnitude of \vec{R}_S is rather small (compared to $|\vec{b}|$), the Burgers vectors of the stair-rod dislocations will be very small in the case of APB tubes formed by APB faults on $\{111\}$ planes. Therefore the influence of these stair-rod dislocations on the contrast of the tube is expected to be weak as proved by image simulations.

The results obtained show that the additional structural component lies in the plane of the APB fault, indicating that in the case of a tube only very small structural changes inside and outside the tube are expected to occur.

V. CONCLUSION

In Ni₃Al deformed at room temperature a high density of APB tubes is observed by TEM methods. Their unexpected contrast occurring in different fundamental reflections is explained by an additional structural displacement vector \vec{R}_S of APB faults on $\{111\}$ planes. This vector lies in the fault plane and is perpendicular to the pure chemical displacement vector \vec{R}_C . \vec{R}_S agrees well with results of calculations of the (111) γ surface in Ni₃Al. In addition, the experiments indicate that contrary to previous models no displacement component perpendicular to the fault planes exists in the case of the tubes.

ACKNOWLEDGMENT

The authors gratefully acknowledge financial support by the Austrian Science Fund.

*URL: <http://www.univie.ac.at/Materialphysik/EM>. Electronic address: Christian.Rentenberger@univie.ac.at

¹A.E. Vidoz and L.M. Brown, *Philos. Mag. A* **7**, 1167 (1962).

²P.M. Hazzledine and P.B. Hirsch, in *High-Temperature Ordered Intermetallic Alloys II*, edited by N. S. Stoloff, C. C. Koch, C. T. Liu, and O. Izumi, Mater. Res. Soc. Symp. Proc. No. 81 (Materials Research Society, Pittsburgh, 1987), p. 75.

³G. Schoeck, *Acta Metall.* **17**, 147 (1969).

⁴P.M. Hazzledine and Y.Q. Sun, *Mater. Sci. Eng., A* **152**, 189 (1992).

⁵C.T. Chou, P.B. Hirsch, M. McLean, and E. Hondros, *Nature (London)* **300**, 621 (1982).

⁶Y.Q. Sun, *Philos. Mag. A* **65**, 287 (1992).

⁷A.H.W. Ngan, I.P. Jones, and R.E. Smallman, *Philos. Mag. B* **67**, 417 (1993).

⁸E. T. Mühlbacher, Master's thesis, University of Vienna, 1993.

⁹X. Shi, G. Saada, and P. Veyssiere, *Philos. Mag. A* **73**, 1159 (1996).

¹⁰C. Lang, C. Rentenberger, and H. P. Karnthaler, in *Proceedings of the 4th Multinational Congress on Electron Microscopy*, edited by K. Kovacs (University of Veszprem, Veszprem, 1999), p. 341.

¹¹H. P. Karnthaler, B. Mingler, C. Rentenberger, and T. Waitz, in *Proceedings of the 12th European Congress on Electron Microscopy 2*, edited by J. Gemperlova and I. Vavra (Czechoslovak Society for Electron Microscopy, Brno, 2000), p. 9.

¹²A.H.W. Ngan, *Philos. Mag. Lett.* **70**, 121 (1994).

- ¹³M. Yamaguchi, V. Vitek, and D.P. Pope, *Philos. Mag. A* **43**, 1027 (1981).
- ¹⁴D. Farkas and E.J. Savino, *Scr. Metall.* **22**, 557 (1988).
- ¹⁵D. Farkas, E.J. Savino, P. Chidambaram, A.F. Voter, D.J. Srolovitz, and S.P. Chen, *Philos. Mag. A* **60**, 433 (1989).
- ¹⁶G. Schoeck, S. Kohlhammer, and M. Fähnle, *Philos. Mag. Lett.* **79**, 849 (1999).
- ¹⁷R. Schäublin and P.A. Stadelmann, *Mater. Sci. Eng., A* **164**, 373 (1993).
- ¹⁸H.P. Karnthaler, C. Rentenberger, and E. Mühlbacher, in *High-Temperature Ordered Intermetallic Alloys V*, edited by I. Baker, R. Darolia, J. D. Whittenberger, and M. H. Yoo, *Mater. Res. Soc. Symp. Proc. No. 288* (Materials Research Society, Pittsburgh, 1993), p. 293.
- ¹⁹B. Grabner, Master's thesis, University of Vienna, 1996.
- ²⁰W. Liu, A. Gemperle, J. Gemperlova, V. Paidar, and E. Nembach, *Acta Mater.* **46**, 6173 (1998).
- ²¹J.M. Sanchez, S. Eng, Y.P. Wu, and J.K. Tien, in *High-Temperature Ordered Intermetallic Alloys II*, edited by N. S. Stoloff, C. C. Koch, C. T. Liu, and O. Izumi, *Mater. Res. Soc. Symp. Proc. No. 81* (Materials Research Society, Pittsburgh, 1987), p. 57.
- ²²C.T. Chou and P.B. Hirsch, *Proc. R. Soc. London, Ser. A* **387**, 91 (1983).
- ²³M. Yamaguchi, D.P. Pope, V. Vitek, and Y. Umakoshi, *Philos. Mag. A* **43**, 1265 (1981).
- ²⁴S. Kohlhammer, M. Fähnle, and G. Schoeck, *Scr. Mater.* **39**, 359 (1998).